

## PAPER

[View Article Online](#)  
[View Journal](#) | [View Issue](#)

Cite this: *Polym. Chem.*, 2025, **16**, 868

# Polyurethane diacrylate incorporated pressure-sensitive adhesives with enhanced strain recovery†

Geonwoo Lee,  ‡, Jinhoon Lee,  ‡, Geonho Lee,  Chihyun Seo, Myung-Jin Baek  and Dong Woog Lee  \*

Pressure-sensitive adhesives (PSAs) are used in a wide range of applications, including electronics, automobiles, healthcare, and packaging, due to their excellent bonding affinity with minimal applied pressure without the need for solvents, heat, or additional processing. Although they exhibit excellent usability with high adhesion strength, PSAs must overcome the limitation of delamination caused by poor strain recovery to be applied to flexible electronics. In this study, we achieved rapid strain recovery in PSAs by utilizing polyurethane diacrylate (PUDA) as a crosslinker. The fabricated PSA demonstrated a significantly faster strain recovery time (~2.5 s) compared to the conventional crosslinked 1,6-hexanediol diacrylate (HDDA) PSA (~61.0 s). Notably, the PUDA PSA also exhibited outstanding 180° peel strength (~22.0 N per 25 mm), surpassing that of a commercial PSA (~12.3 N per 25 mm). The fabricated PSAs showed promise for applications under harsh straining conditions confirmed through 100 strain-recovery cycles at 20% tensile strain. This study directs the way to improve PSA's poor strain recovery properties and paves the way for the future advancement direction in adhesive technology.

Received 27th September 2024,  
Accepted 31st December 2024

DOI: 10.1039/d4py01084a

[rsc.li/polymers](https://rsc.li/polymers)

## Introduction

The electronic device market has undergone a significant transition in response to versatile forms of devices, replacing the traditional bar-shaped rigid devices with adaptable and flexible designs.<sup>1–4</sup> To enhance the devices' marketability and user-accessibility, developing wearable devices<sup>2,5</sup> and foldable displays<sup>6–8</sup> is of great interest. These devices can change their forms freely with bending or twisting motions; therefore, transitioning traditional rigid electronic components into more flexible ones is required.<sup>9</sup> For example, displays are usually composed of a protection film, cover glass, a light-emitting layer, a back film, a circuit plate, and more, which are also essential in flexible displays. Furthermore, these components are assembled with optically clear PSAs due to their flexibility and strong adhesion strength.<sup>10–13</sup> Therefore, developing optically clear PSAs with excellent strain recoverability is one of the main hurdles in flexible device manufacturing.

Recent studies on PSAs have primarily focused on enhancing their adhesion strength<sup>14,15</sup> under straining conditions. However, for the frequently shape-changing devices, the PSAs

should maintain their flexibility and further exhibit rapid recovery properties against strain. To address this, various studies have explored the methods to improve the strain recovery performance of PSAs.<sup>16–19</sup> Despite these advancements, the complex fabrication process and high costs are still challenging for the commercialization of PSAs. Therefore, there are growing demands for cost-effective adhesives, which possess both excellent adhesion strength and strain recovery properties.

Polyurethanes (PUs), a class of polymers characterized by urethane bonds, are typically synthesized through the reaction of polymeric isocyanates with polyols.<sup>20</sup> Due to their versatility, they are widely used across various industries in applications such as coatings,<sup>21–23</sup> adhesives,<sup>24–26</sup> and sealants.<sup>27</sup> The elasticity of polyurethanes is attributed to the microphase separation between the hard and soft segments in the polymer chains.<sup>28,29</sup> The polyol segments, generally consisting of linear organic chains, contribute to the polymer softness, while the isocyanate segments provide rigidity. PU additives are known for not only their elasticity but also their versatility. Therefore, several studies were conducted to utilize PUs in PSAs to provide various functions, for instance, modulating viscoelastic properties or hardness of polymers<sup>30,31</sup> and providing stability under heat condition with silane-terminated PU.<sup>32</sup>

In this work, we synthesized acrylic PSAs utilizing commercially available polyurethane diacrylate (PUDA) as a crosslinker to enhance strain-recovery properties. Various compositions of PUDA-crosslinked PSAs were prepared by adjusting the

School of Energy & Chemical Engineering, UNIST (Ulsan National Institute of Science and Technology), Ulsan, 44919, Republic of Korea.

E-mail: [dongwoog.lee@unist.ac.kr](mailto:dongwoog.lee@unist.ac.kr)

† Electronic supplementary information (ESI) available. See DOI: <https://doi.org/10.1039/d4py01084a>

‡ These authors contributed equally to this work.

amount of crosslinker and their adhesive, optical, and mechanical properties were evaluated. Our results showed that PUDA-crosslinked PSAs exhibited superior strain-recovery properties compared to control PSAs crosslinked with 1,6-hexanediol diacrylate (HDDA) at equivalent crosslinker concentrations. While the adhesion performance and optical transmittance were comparable between PUDA and HDDA PSAs, the strain-recovery properties were notably improved in the PUDA PSAs. Additionally, increasing the PUDA crosslinker concentration resulted in a reduction in strain recovery times. These findings suggest that PUDA-crosslinked PSAs possess high potential for flexible electronic devices which are exposed to multimodal and frequent deformation.

## Results and discussion

### Characterization of synthesized PSAs

To synthesize the PSAs, we fixed the monomer ratio of 2-ethylhexyl acrylate (2-EHA) and 2-carboxyethyl acrylate (2-CEA) at 70:30 mol%, following a previous study.<sup>15</sup> Various adhesive samples were prepared by adjusting the amount of PUDA crosslinker. These samples were named *x* PUDA, where *x* represents the mol% of the PUDA crosslinker in the monomer mixture. Specifically, samples containing 0.1 mol%, 0.15 mol%, 0.2 mol%, and 0.4 mol% PUDA were prepared and labeled accordingly as 0.1 PUDA, 0.15 PUDA, 0.2 PUDA, and 0.4 PUDA. A sample incorporating 0.15 mol% of the HDDA crosslinker, labeled 0.15 HDDA, was also prepared to compare the performances of the PUDA-based samples.

The PUDA crosslinker's functional groups are analyzed by nuclear magnetic resonance (NMR) spectroscopy using a 600 MHz FT-NMR spectrometer (AVANCE NEO 600, Bruker, USA). In the <sup>1</sup>H NMR spectrum (Fig. S1†), peaks appear in the 5.8–6.5 ppm region, which indicates the presence of hydrogens in the acrylate group. Additionally, in the <sup>13</sup>C NMR spectrum (Fig. S2†), the a peak indicates the carbon in the acrylate group. Therefore, we confirmed that the utilized PUDA (PU2100, Miwon Specialty Chemical Co., Ltd) contained an acrylate group. Also, through the b and c peaks in the <sup>13</sup>C NMR spectrum, we confirmed that PUDA contains urethane bonds.

The thermal properties of the prepared PSAs were investigated. The glass transition temperatures (*T<sub>g</sub>*) of the PSAs were determined using differential scanning calorimetry (DSC). As shown in Fig. S4,† the *T<sub>g</sub>* values for the samples containing 0.1, 0.15, 0.2, and 0.4 mol% PUDA were measured at −35.5 °C, −36.8 °C, −38.2 °C, and −39.2 °C, respectively. These values, significantly lower than room temperature, suggest that the prepared adhesives can be used under ambient conditions. The decrease in *T<sub>g</sub>* with increasing crosslinker concentration can be attributed to the higher free volume provided by the long PUDA crosslinker (*M<sub>w</sub>* ~ 1400 g mol<sup>−1</sup>).<sup>33,34</sup>

Additionally, the thermal stability of each sample was confirmed through thermogravimetric analysis (TGA). As shown in Fig. S5,† two degradation temperatures were observed, around

180 °C and 350 °C. The first degradation temperature, around 180 °C, is attributed to the cleavage of the ether bonds in the CEA molecules. From the second degradation point, it was revealed that all samples exhibited a high 50% degradation temperature (*T<sub>50d</sub>*) of approximately 385 °C. Also, the degradation temperature is much higher than the operation temperature of general displays, which ranges from −40 °C to 85 °C.<sup>35</sup> Therefore, the prepared PSAs demonstrate sufficient thermal stability at high temperatures, making them suitable for use in various free-form devices.

Furthermore, the rheological properties of the PSAs were evaluated to determine their applicability using the Chang window for PSAs, through a frequency sweep from 0.1 Hz to 100 Hz using a rheometer.<sup>36–38</sup> In brief, the Chang window allows the potential applications of PSAs to be determined based on their rheological properties. Depending on which quadrant of the Chang window the values of *G'* and *G''* fall within, across the frequency range 1 Hz to 100 Hz, their application can be identified. As shown in Fig. 1a, a significant increase in storage modulus (*G'*) was observed as the crosslinker concentration increased. Additionally, as *G'* increases, the loss modulus (*G''*) also increases with higher crosslinker concentration, indicating an increase in crosslinking density (Fig. 1b). We then plotted the *G'* values of the PSA samples against *G''*, as shown in Fig. 1c. In Fig. 1d, the *G'–G''* graph was overlapped with the Chang window, showing that the synthesized PSAs may be used for various applications except as high-tack PSAs. At lower crosslinker concentrations, the PSAs were positioned in quadrant 3 of the Chang window, indicating their potential applicability as removable PSAs. As the crosslinker concentration increased, both the storage modulus and loss modulus also increased, shifting the results towards the center (general purpose PSAs) and quadrant 2 (high performance PSAs) of the Chang window. Therefore, PUDA-based PSAs are expected to be applicable in various fields depending on the crosslinker concentration.

### Adhesive properties of synthesized PSAs

The adhesive strengths of the synthesized pressure-sensitive adhesives (PSAs) were quantitatively evaluated using the ASTM D3330 Method A—180° peel adhesion test, conducted on a universal testing machine (UTM) with a 10 kg load cell, as shown in Fig. 2a.

The results shown in Fig. 2b, indicate that the 0.1 PUDA sample exhibited the highest 180° peel strength among the PUDA series with a value of 29.1 ± 3.0 N per 25 mm, which is comparable or higher than those in previous studies conducted with carboxylic acid containing monomers.<sup>14,15,18,39–47</sup> As the concentration of the crosslinker increased, a decrease in adhesive strength was observed. This decrease in adhesion strength can be attributed to increased crosslinking within the acrylic polymer chains, which reduces the availability of hydrogen bonding sites on the surface, leading to decreased adhesion. Furthermore, the adhesion strength of the 0.1 PUDA sample, measuring 28.9 ± 2.1 N per 25 mm, was comparable to

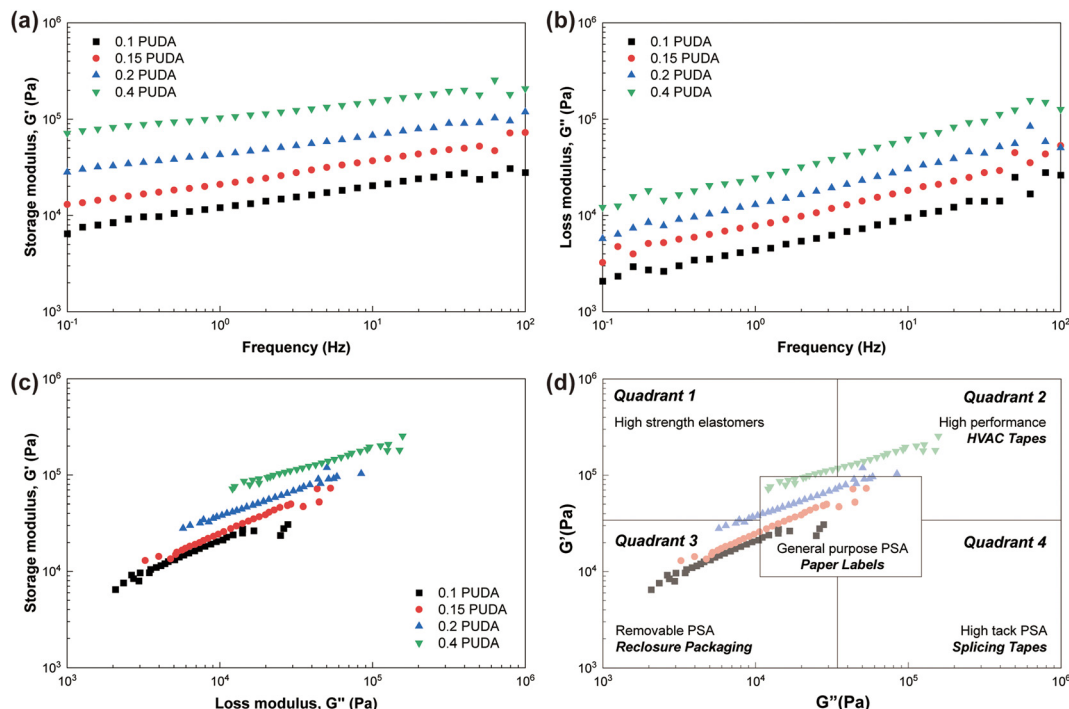


**Fig. 1** Rheological properties of PSA samples. (a) The storage modulus ( $G'$ ) and (b) the loss modulus ( $G''$ ) of the PU DA PSAs with the rheometer's frequency sweep. (c) The PU DA PSAs'  $G'$ - $G''$  graph. (d) The overlap of the  $G'$ - $G''$  graph and the Chang window which is the basis for determining PSA's applicability.

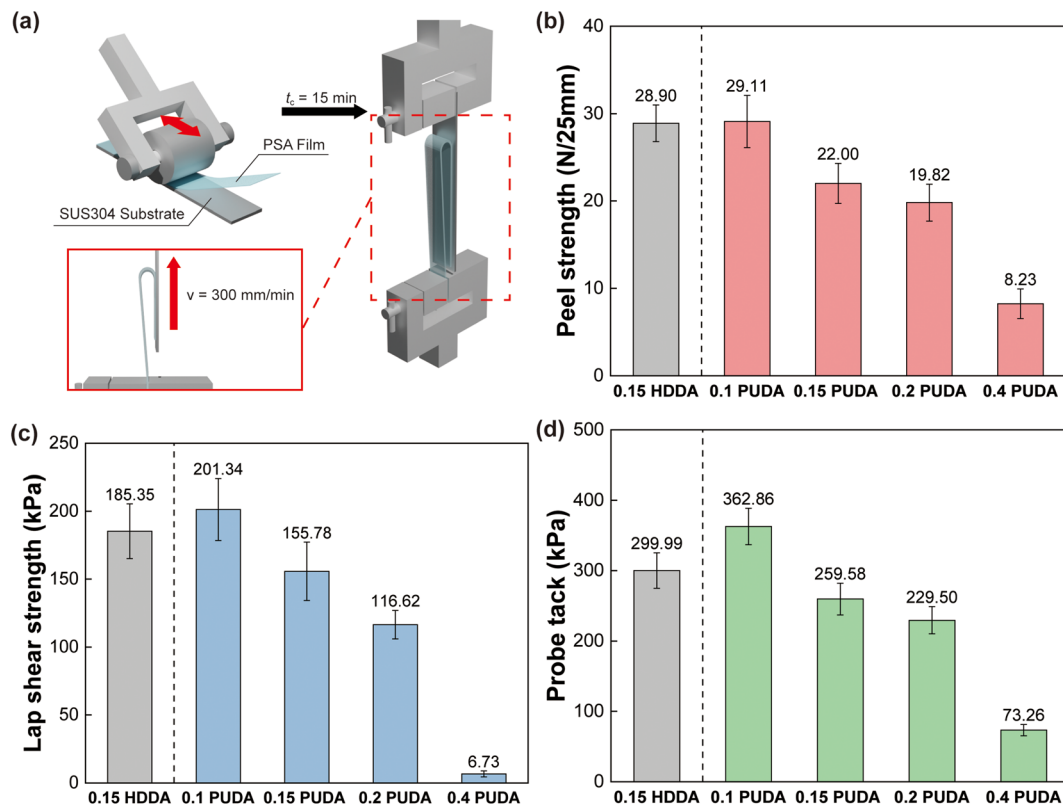


**Fig. 2** Adhesion properties of PSA samples. (a) Adhesion strength measurement process (ASTM D3330 method A). (b) 180° peel strength, (c) lap shear strength, and (d) probe tack results of the prepared samples. The resulting values were confirmed by at least 3 times repeated tests.

that of the control PSA containing 0.15 mol% of the HDDA crosslinker.

In addition to the 180° peel adhesion test, the lap shear test (Fig. 2c) and probe tack test (Fig. 2d) further confirmed the adhesive properties of the PUDA-based PSAs. Through the lap shear test, we demonstrated that PUDA-based PSAs possess strong cohesive strength, making them suitable for applications requiring long-term adhesion stability under shear stress. On the other hand, the probe tack test, which measures the tackiness or stickiness of the PSA when lightly pressed and quickly removed, revealed that PUDA-based PSAs maintain excellent initial adhesion performance. This characteristic is essential for applications where immediate bonding on contact is critical. Overall, the PUDA-based PSAs exhibited a well-balanced performance in both adhesion strength and mechanical durability, comparable to conventional HDDA-based PSAs.

### Mechanical property tests

The mechanical properties of the prepared samples were evaluated using a UTM. The stress-strain curves of the samples are shown in Fig. S6,† and the specific mechanical parameters, including Young's modulus, toughness, ultimate tensile strength, and elongation at break, are presented in Fig. 3. As the crosslinker content increased, Young's modulus (Fig. 3a) also increased, indicating that the samples became stiffer and

more resistant to strain. This increase in Young's modulus can be attributed to the higher density of crosslinking, which makes the samples structurally stiffer.

Despite the higher PUDA content, there was a significant decrease in both toughness (Fig. 3b) and elongation at break (Fig. 3c). These findings can be explained by considering the relationship between Young's modulus and ultimate tensile strength (Fig. 3d). While the stiffness of the samples increased with higher crosslinking, the ultimate tensile strength remained relatively unchanged. This is because ultimate tensile strength is more influenced by the backbone structure of the polymer chains rather than crosslinking density.<sup>48,49</sup>

As the crosslinking density increases, the samples become stiffer, which causes them to reach their ultimate tensile strength at lower strains. Consequently, the elongation at break decreases with increasing PUDA content, and the overall toughness of the sample also declines as the elongation at break decreases.

### Stress-relaxation and strain-recovery tests

The stretchability and recovery properties of the samples were characterized through stress-relaxation and strain-recovery tests under varying strain levels (10%, 20%, 50%, and 100%), using a UTM. First, the samples were strained to each strain level, and the stress was recorded over time (Fig. 4a). After 15 minutes, the applied strain was released, and the deformed

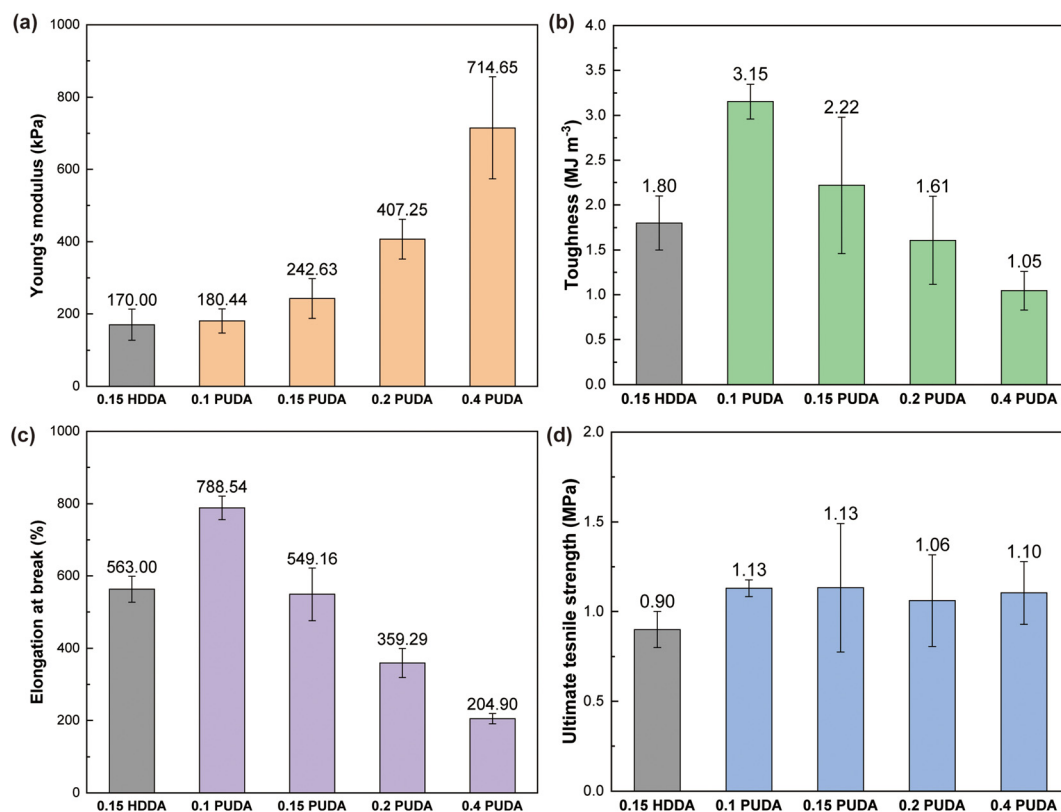


**Fig. 3** Mechanical properties of prepared PSAs. (a) Young's modulus, (b) toughness, (c) elongation at break, and (d) ultimate tensile strength of each PSAs. Result values were confirmed by at least 3 times repeated tests. 0.15 HDDA sample's results are obtained from ref. 18.

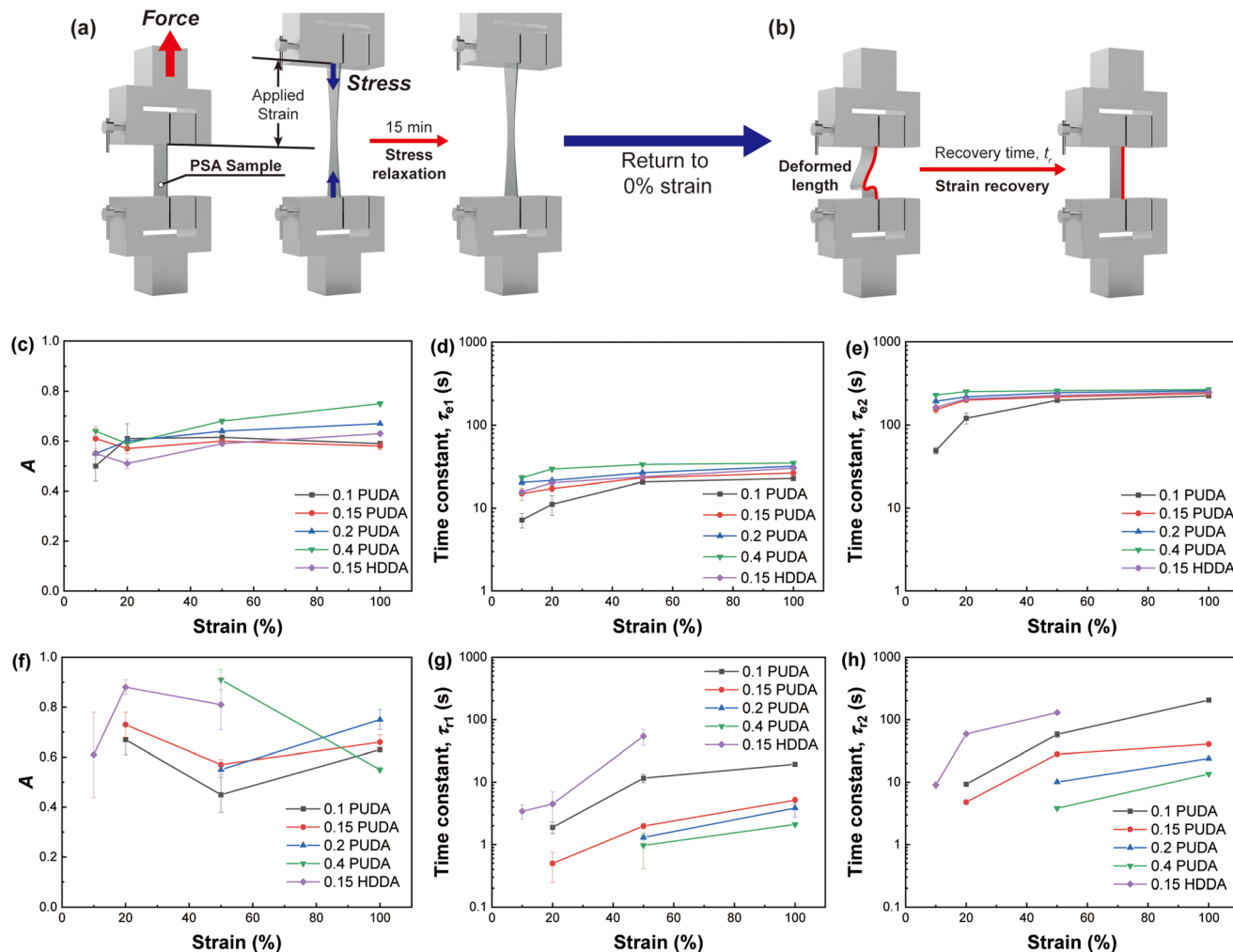


**Fig. 4** The experimental schematic of (a) stress relaxation and (b) strain recovery test. In stress relaxation, each sample is strained to 10, 20, 50, and 100% of original length. After stretching, the stress applied to the sample was measured until 15 min. After 15 min, the sample's strain returned to 0% and the stretched sample's length was measured. Fitting parameters of (c)–(e) normalized stress relaxation curves and (f)–(h) normalized strain recovery curves. Fittings were conducted with double exponential decay and normalization was conducted with min–max normalization ( $\bar{a} = (a - a_{\min})/a_{\max}$ ).

length of each sample was measured over time as it returned to its original length (Fig. 4b).

The results of the stress-relaxation test are plotted in Fig. 5. In all samples, applied stress relaxed rapidly at the initial point, and gradually reached a plateau over time. Additionally, as the strain increased, the stress value at the 0 second also increased, following the same trend observed in the stress-strain curve, and the stress increased when they reached the relaxation plateau. However, the each sample's stress-relaxation ability cannot be fully evaluated from these time–stress curves. To gain a better understanding of the stress-relaxation behavior, the data were analyzed using a double exponential decay model (eqn (1)) after applying min–max normalization.

$$\bar{\sigma} = A \cdot e^{-t/\tau_{e1}} + (1 - A) \cdot e^{-t/\tau_{e2}}, \quad (1)$$

Here,  $A$  is the proportionality constant, and  $\tau_{e1}$  and  $\tau_{e2}$  are the first and second stress relaxation time constants, respectively.

$\tau_{e1}$  and  $\tau_{e2}$  are time constants related to several stress relaxation mechanisms in the transient and prolonged time ranges, respectively. These mechanisms include chain disentanglement, viscous flow, molecular interactions, or bond interchange in physical crosslinking.<sup>14,50–53</sup> As shown in Fig. 4c, the  $A$  does not vary significantly with changes in the crosslinker type or concentration. Fig. 4d and e show that the 0.1 PUDA and 0.15 PUDA samples have lower  $\tau_{e1}$  and  $\tau_{e2}$  compared to the 0.15 HDDA sample. This result suggests that the 0.1 PUDA and 0.15 PUDA samples exhibit faster stress-relaxation. As the concentration of the crosslinker increased, the time constants also increased, which indicates that higher crosslinking density leads to slower stress relaxation.

The strain-recovery test results are shown in Fig. 6. All of the samples could fully recover their strain under the 50% strain for 15 min. Also, in contrast to the 0.15 HDDA sample, 0.1, 0.15, and 0.2 PUDA samples show strain recovery even at 100% strain during 15 min. In the case of 0.4 PUDA, full strain



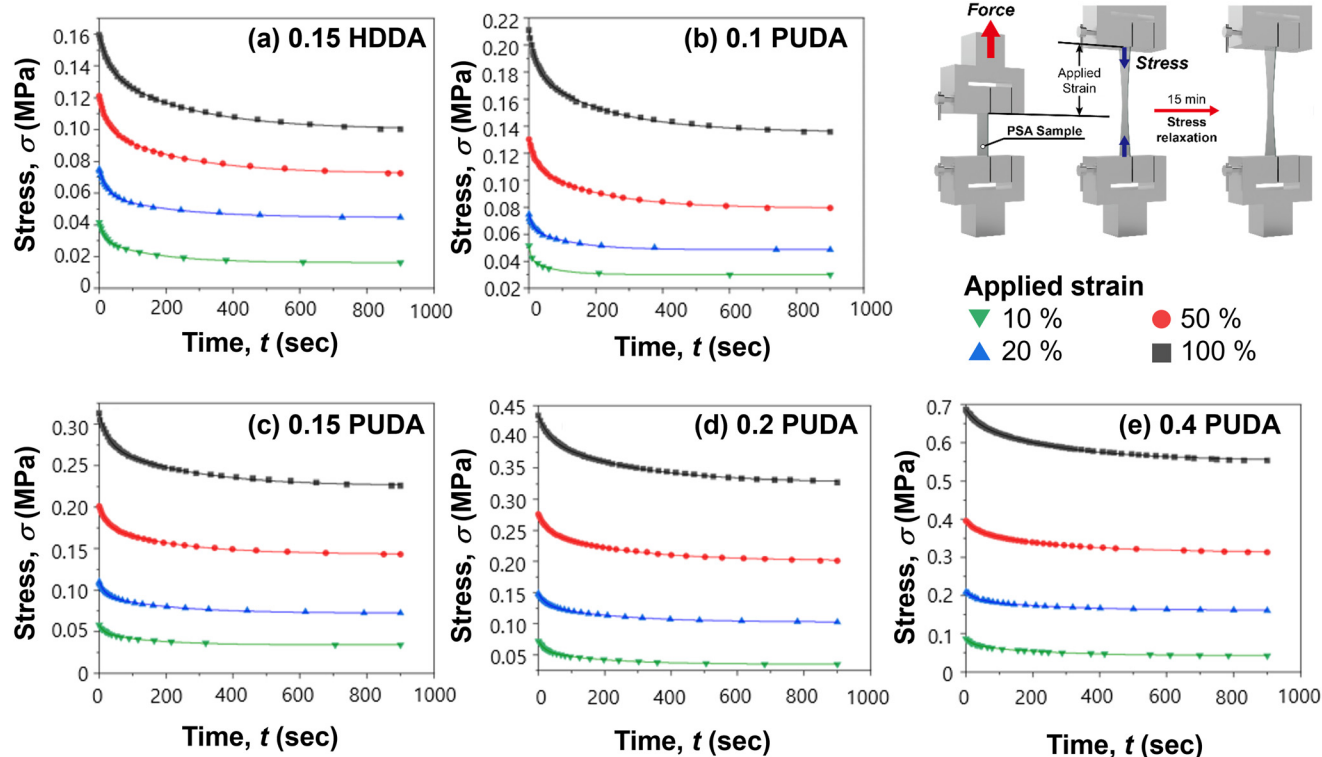


Fig. 5 Stress relaxation curve of PSA crosslinked with (a) 0.15 mol% HDDA, (b) 0.1 mol% PUDA, (c) 0.15 mol% PUDA, (d) 0.2 mol% PUDA, and (e) 0.4 mol% HDDA during 15 min.

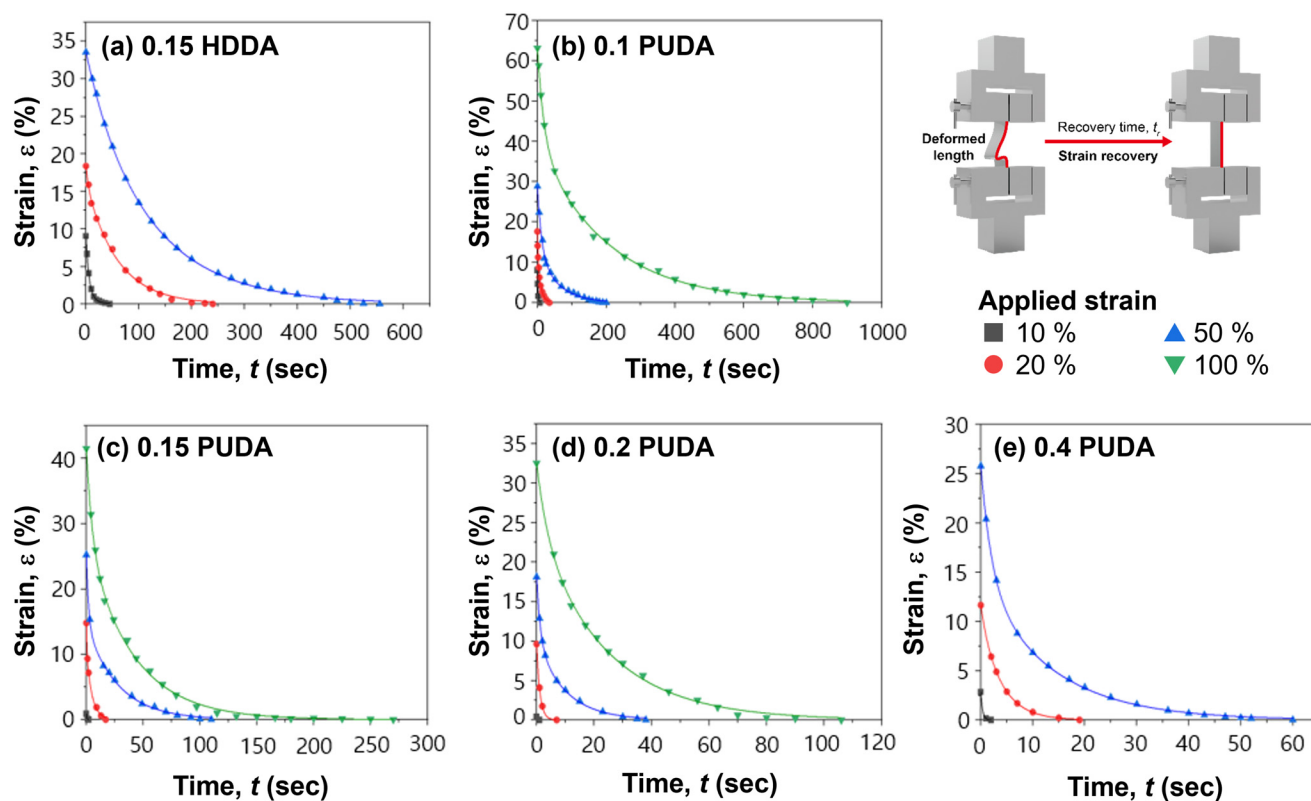


Fig. 6 Strain-recovery curve of PSA crosslinked with (a) 0.15 mol% HDDA, (b) 0.1 mol% PUDA, (c) 0.15 mol% PUDA, (d) 0.2 mol% PUDA, and (e) 0.4 mol% HDDA.

recovery did not occur under 100% straining conditions due to the lower yield strain. The strain recovery abilities cannot be fully evaluated from the time-strain curve. Therefore, to evaluate the strain-recovery properties of each sample more accurately, the results were analyzed using double exponential decay fitting (eqn (2)) after min-max normalization.

$$\bar{\varepsilon} = A \cdot e^{-t/\tau_{r1}} + (1 - A) \cdot e^{-t/\tau_{r2}}, \quad (2)$$

Here,  $A$  is the proportionality constant, and  $\tau_{r1}$  and  $\tau_{r2}$  are the first and second strain recovery time constants, respectively.  $\tau_{r1}$  is related to the strain-recovery due to the original network structure mostly due to chain motion and orientation such as uncoiling, disentangling, and rupture of the microdomain,<sup>54</sup> and  $\tau_{r2}$  is related to prolonged strain-recovery due to the weak noncovalent bonds mostly due to the dynamically formed hydrogen bonding network.<sup>55,56</sup>

In the strain-recovery results, the proportionality constant  $A$  (Fig. 4f) does not show significant variation with the crosslinker type, similar to stress-relaxation. However, in Fig. 4g and h, both time constants for the PUDA samples are significantly lower than those for the HDDA sample, indicating faster strain-recovery properties. Additionally, the time constants decrease rapidly with increasing PUDA concentration, suggesting that the higher cross-linking density helps PSA to maintain its original network structure with minimal reformation of hydrogen bonding upon straining.

As a result, we conclude that PSAs with PUDA crosslinkers exhibit exceptional strain-recovery properties along with fast stress-relaxation.

### Repetitive strain-cycle test

The strain recovery properties of the samples were evaluated by measuring the recovery time after 100 repetitive strain cycles. In brief, the samples were strained to 20% of their original length and then released immediately, with this cycle repeated 100 times. During the 100 cycles, stress-strain curves were recorded (Fig. 7a–e).

Firstly, as the concentration of the PUDA crosslinker increased, higher stress was observed at 20% strain, which aligns with the Young's modulus values obtained from the tensile stress-strain curves (Fig. 3a). Additionally, the hysteresis observed in the stress-strain curves changed with varying crosslinker concentrations. At lower crosslinker concentrations, a peak around 2.5% strain was observed during the straining phase. In the 0.2 PUDA sample, this peak's height decreased, and in the 0.4 PUDA sample, the peak disappeared. This peak was due to the maintained stretched length of the sample after release. Therefore, as the crosslinker concentration increases, the faster strain-recovery property results in reduced hysteresis in the stress-strain curve.

After 100 strain cycles, the recovery time of the strained samples was measured until they returned to their original length. As shown in Fig. 7f, the 0.15 HDDA sample, which does not contain urethane bonding, had a recovery time of 61 seconds after 100 strain cycles. In contrast, all samples containing urethane bonding demonstrated significantly shorter recovery times compared to the 0.15 HDDA sample. Even the 0.1 PUDA sample, which had fewer crosslinking sites than the 0.15 HDDA sample, exhibited a recovery time that was approxi-

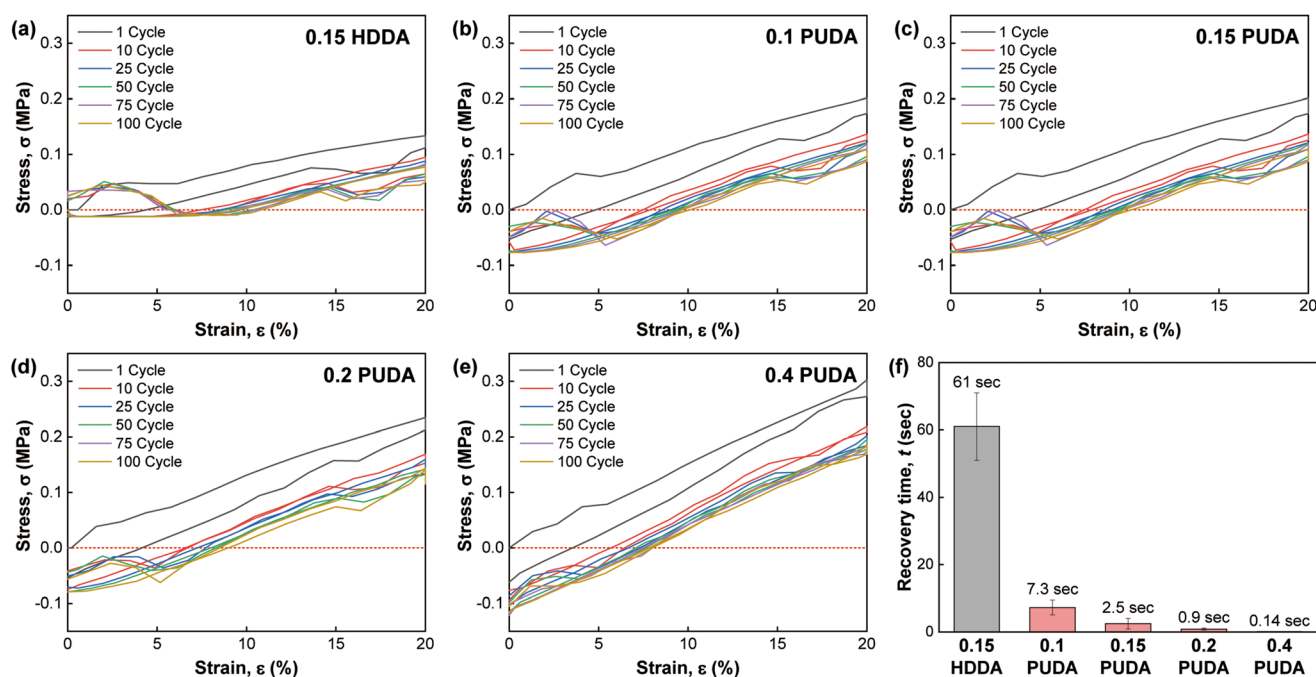
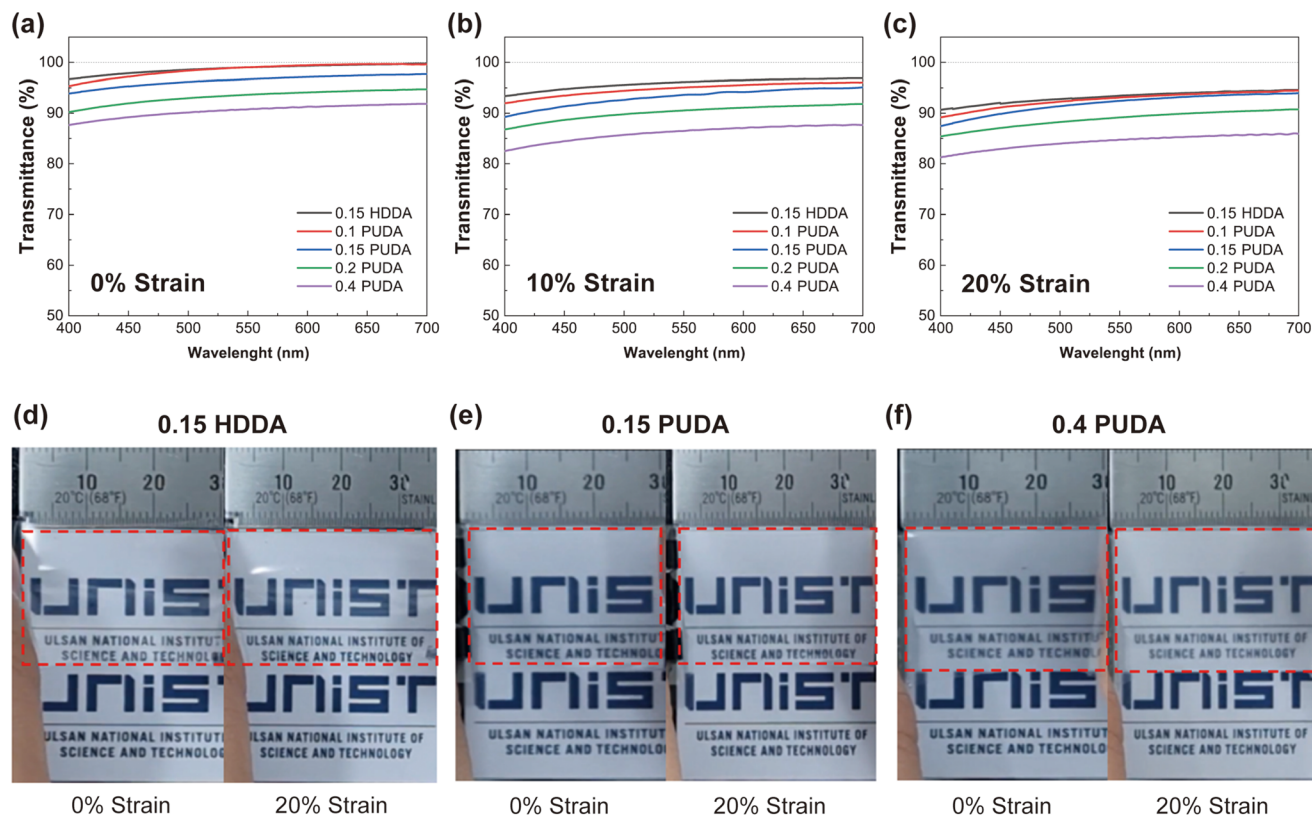


Fig. 7 (a)–(e) 100 times repetitive strain test with a 20% strain-return cycle of each sample. As the concentration of the crosslinker increases, the stress-strain curve shows a stiffer slope and higher stress at 20% strain. (f) The strain recovery time after 100 strain-return cycles.



**Fig. 8** (a)–(c) Optical transmittance properties of each sample with various strains. Transmittance of each sample was measured by UV-Vis spectroscopy. Also, strained samples were attached on slide glass with each strain. 100% transmittance is noted as a black dotted line. (d)–(f) Optical image of each sample with 0% and 20% strains. Samples are marked with a red dashed box on each image. Original length of the samples is 30 mm. Also, after strain, each sample maintains the transmittance and clear properties.

mately 88% shorter. As the crosslinker content increased, the recovery time of the samples decreased. This is due to the increased crosslinking sites enhancing the sample's elasticity, leading to quicker recovery.

These results suggest that PSAs with PUDA crosslinkers have excellent strain-recovery properties and could be effectively used in various free-form devices subjected to frequent strain and release conditions, such as foldable, rollable, and stretchable devices.

### Optical transmittance test

For potential applications as display laminating materials, it is crucial for PSAs to exhibit high optical transmittance in the visible light range. To assess this property, UV-Vis spectroscopy was conducted in the visible light region. The results, shown in Fig. 8a, indicate that, under no strain conditions, most PSA samples maintained a transmittance of over 90% across the visible light range.

Additionally, as illustrated in Fig. 8b and c, the transmittance decreased when the samples were strained due to the increase in crystallinity. Therefore, as the strain increases, the polymer chains in the PSA film aligned along the longitudinal direction, leading to a decrease in transmittance. Nevertheless, the 0.1 PUDA sample still retained a high transmittance above

90% with various strain conditions. The high optical clarity of the samples under various strains was further confirmed through optical imaging (Fig. 8d–f). The images on the backside of the strained PSA samples remained clearly visible, demonstrating the adhesive's ability to maintain clarity and visibility under different physical conditions. This observation highlights the suitability of these adhesives for use in display lamination, where maintaining high optical clarity and visibility is essential.

## Conclusions

The synthesized pressure-sensitive adhesives (PSAs), particularly those incorporating PUDA crosslinkers, exhibit promising properties for advanced applications in flexible and free-form electronic devices. The evaluation of adhesion properties revealed that as the concentration of PUDA crosslinkers increased, adhesion strength decreased. However, the 0.1 PUDA and 0.15 PUDA samples show excellent adhesion strength which is comparable to that of the 0.15 HDDA sample.

In terms of strain recovery, the PUDA crosslinked PSAs demonstrated superior performance compared to the HDDA



PSA sample. The faster stress-relaxation decay times and reduced strain-recovery time highlight the improved flexibility and rapid strain recovery of the PUDA PSAs. The 100-cycle strain-recovery test further supported these findings, showing that PUDA crosslinked samples recovered significantly faster than HDDA crosslinked samples.

Optical transmittance tests confirmed that the PSAs, particularly the 0.1 PUDA sample, maintained high clarity with transmittance exceeding 90% even under strain. This high optical clarity was further validated by optical imaging, which showed that images remained visible through the strained samples, underscoring their suitability for display lamination applications.

Overall, the study demonstrates that PSAs with PUDA crosslinkers offer a desirable balance of mechanical flexibility, rapid strain recovery, and excellent optical clarity. These properties make them well-suited for use in flexible electronic devices, such as foldable, rollable, and stretchable displays, where durability, performance under strain, and high visibility are essential.

## Experimental section

### Materials

2-Ethylhexyl acrylate (EHA) and 2-carboxyethyl acrylate (CEA) were purchased from Sigma-Aldrich. The photoinitiator, phenylbis(2,4,6-trimethylbenzoyl)phosphine oxide (BAPO), was purchased from TCI chemicals. 1,6-Hexanediol diacrylate (HDDA) was purchased from Alfa Aesar. The PUDA crosslinker, PU2100, was obtained from Miwon Specialty Chemical Co., Ltd. The hydrophobic fumed silica (Aerosil R974) was purchased from Evonik Industries. The poly(ethylene terephthalate) (PET) film (SH82) and releasing film (SG31) were purchased from SKC. All reagents were used without any pre-treatment process.

### Preparation of pressure sensitive adhesives (PSAs)

The PSAs were prepared with the following methods. First, EHA and CEA which are acrylate monomers were mixed in a 70:30 (mol%) ratio. As crosslinkers, PUDA and HDDA were added into the monomer mixture in different ratios (Table 1). The viscosity of the mixtures was adjusted by adding 15 phr of hydrophobic fumed silica to coat with the blade coating method. 0.1 mol% of the photoinitiator (BAPO) was added into the mixture and mixed using a vortex mixer.

**Table 1** Crosslinker ratios of PSAs. Monomer ratios were fixed to 70:30 mol% of EHA and CEA. All samples include the same amount of photoinitiator (0.1 mol%) and fumed silica (12 phr; per hundred resin)

mol%	0.15 HDDA	0.1 PUDA	0.15 PUDA	0.2 PUDA	0.4 PUDA
HDDA	0.15	—	—	—	—
PUDA	—	0.1	0.15	0.2	0.4

To make samples for adhesion property measurements, the prepared mixtures were coated on a PET film (SH82) and covered with a releasing film (SG31) using a blade coating device (KP-3000VH, KIPAE, South Korea). To test the mechanical properties of PSAs, the prepared mixtures were coated between releasing films (SG31) with the same methods. After the coating process, the prepared films were cured with conveyor UV curing devices with 365 nm, 1 W cm<sup>-2</sup> at a 50 mm distance for 1 min. The thickness of cured PSA films was 100 ± 10 µm.

### Characterization of the prepared PSAs

The glass transition temperatures ( $T_g$ ) were measured using differential scanning calorimetry (DSC) (Q200, TA Instrument, USA) under a nitrogen atmosphere with a 5 °C min<sup>-1</sup> scanning rate from -60 °C to 120 °C. To assess thermal stability, the weight loss of the sample with the temperature increase was measured by thermogravimetric analysis (TGA) (Q400, TA Instrument, USA) under a nitrogen atmosphere with a 10 °C min<sup>-1</sup> heating rate, from 40 °C to 600 °C. The rheological characteristics of the samples were conducted with a rheometer (Kinexus Pro+, NETZSCH, Germany). The samples were prepared with about 10 mm radius and sandwiched between removable PET films on both sides. Before the test, the removable PET films were removed. The rheological properties were tested using frequency sweep mode with the frequency ranging from 0.1 to 100 Hz and 0.025% strain at room temperature. The applied normal force was set to 3 N and a PU20 flat type geometry was used.

### Adhesion property measurements

The 180° peel strength of PSA was determined following the ASTM D3330 method. 25 mm × 100 mm PSA films were prepared and attached to acetone cleaned stainless steel (SUS 304) panels. Then the attached PSAs were pressed using a 2.5 kg hand roller with a 10 mm s<sup>-1</sup> speed twice. After 15 min of pressing, the attached PSA films were peeled using a universal testing machine (UTM) (WL2100C, Withlab, South Korea) at a 300 mm min<sup>-1</sup> crosshead speed. After the peel strength record, the data from the middle 50% of the recorded range, between 25% and 75%, were used to calculate the average peel strength for each sample. Each sample was tested at least 5 times to confirm repeatability.

The lap shear test was conducted using UTM. PSA films were prepared with a 12.7 mm × 12.7 mm shape, and attached between SUS 304 plates. After attachment, the samples were pressed using a 2.5 kg hand roller with a 10 mm s<sup>-1</sup> speed a single time. After 15 min, lap shear stress test was conducted with a 1.3 mm min<sup>-1</sup> crosshead speed.

The probe tack test was conducted using a texture analyser (TXA, Yeonjin, South Korea). A cylindrical probe made of SUS 304 with a 5 mm diameter approaches the PSA films with a 100 mm s<sup>-1</sup> speed. When 100 gf of load was applied to the probe, the probe and PSA were in contact for 1 s, after which the probe was released from the PSA with a 10 mm s<sup>-1</sup> speed.

### Mechanical property tests

Tensile tests were conducted using a universal testing machine (UTM, WL2100C, Withlab, South Korea) with a 300 mm s<sup>-1</sup> crosshead speed at room temperature. The test specimen's size was 12.5 mm × 25 mm after mounting to the universal testing machine. All samples' mechanical properties were analysed with measured stress-strain curves.

### Stress-relaxation and strain-recovery tests

Stress-relaxation and strain recovery properties were measured with a universal testing machine (DAO-u1, DAO Technology, South Korea) with the same specimen size using a tensile test. Each PSA was stretched to 10, 20, 50 and 100% for the stress-relaxation test and the stress was measured for 15 minutes after stretching. The measured stress ( $\sigma$ ) was normalized with min-max normalization with the following eqn (3).

$$\bar{\sigma} = \frac{\sigma - \sigma_{\min}}{\sigma_{\max} - \sigma_{\min}} \quad (3)$$

The strain recovery test was conducted immediately after the stress-relaxation test. After stress-relaxation test, the sample's strain returned to 0% and the sample's total length was measured from the sideview. The length of the bent or deformed PSA was tracked until it reached the steady state, where the length does not change further.

The strain recovery cycle test was conducted with a universal testing machine (DAO-u1, DAO Technology, South Korea). For 100 cycles, PSAs were stretched to 20% strain and relaxed to 0% strain immediately with a 500 mm min<sup>-1</sup> crosshead speed. During the test, strain forces were recorded with a 10 kgf load cell.

### Optical property measurements

Transmittances of PSA films were measured by UV-Vis spectroscopy (V-750, Jasco, Japan). 100  $\mu$ m thickness PSA films were attached to a slide glass (Marienfeld, Germany) with 0, 10 and 20% strain. The prepared samples were placed on a film holder accessory (FLH-740, Jasco, Japan) and transmittance was recorded from 400 nm to 700 nm wavelength, which is the visible light region.

## Author contributions

Geonwoo Lee and Jinhoon Lee: conceptualization, investigation, validation, formal analysis, data curation, and writing – original draft. Geonho Lee, Chihyun Seo, and Myung-Jin Baek: formal analysis and validation. Dong Woog Lee: conceptualization, formal analysis, writing – review & editing, supervision, and funding acquisition.

## Data availability

The data supporting this article have been included as part of the ESI.†

## Conflicts of interest

There are no conflicts of interest to declare.

## Acknowledgements

This research was supported by the Basic Science Research Program (NRF-2023R1A2C2004762) through the National Research Foundation of Korea (NRF), funded by the Ministry of Science and ICT, and the Institute of Civil Military Technology cooperation (No. 22-CM-BR-14) funded by the Defense Acquisition Program Administration and Ministry of Trade, Industry and Energy of Korea government.

## References

- 1 S.-H. Byun, J. Y. Sim, Z. Zhou, J. Lee, R. Qazi, M. C. Walicki, K. E. Parker, M. P. Haney, S. H. Choi, A. Shon, G. B. Gereau, J. Bilbily, S. Li, Y. Liu, W.-H. Yeo, J. G. McCall, J. Xiao and J.-W. Jeong, *Sci. Adv.*, 2019, 5, eaay0418.
- 2 S. Wang, J. Xu, W. Wang, G.-J. N. Wang, R. Rastak, F. Molina-Lopez, J. W. Chung, S. Niu, V. R. Feig, J. Lopez, T. Lei, S.-K. Kwon, Y. Kim, A. M. Foudeh, A. Ehrlich, A. Gasperini, Y. Yun, B. Murmann, J. B. H. Tok and Z. Bao, *Nature*, 2018, 555, 83–88.
- 3 D.-H. Kim, N. Lu, R. Ma, Y.-S. Kim, R.-H. Kim, S. Wang, J. Wu, S. M. Won, H. Tao, A. Islam, K. J. Yu, T.-i. Kim, R. Chowdhury, M. Ying, L. Xu, M. Li, H.-J. Chung, H. Keum, M. McCormick, P. Liu, Y.-W. Zhang, F. G. Omenetto, Y. Huang, T. Coleman and J. A. Rogers, *Science*, 2011, 333, 838–843.
- 4 M. Kaltenbrunner, T. Sekitani, J. Reeder, T. Yokota, K. Kuribara, T. Tokuhara, M. Drack, R. Schwödiauer, I. Graz, S. Bauer-Gogonea, S. Bauer and T. Someya, *Nature*, 2013, 499, 458–463.
- 5 R. Tajima, T. Miwa, T. Oguni, A. Hitotsuyanagi, H. Miyake, H. Katagiri, Y. Goto, Y. Saito, J. Goto, M. Kaneyasu, M. Hiroki, M. Takahashi and S. Yamazaki, *J. Soc. Inf. Disp.*, 2014, 22, 237–244.
- 6 S. Hong, C. Jeon, S. Song, J. Kim, J. Lee, D. Kim, S. Jeong, H. Nam, J. Lee, W. Yang, S. Park, Y. Tak, J. Ryu, C. Kim, B. Ahn and S. Yeo, *SID Symp. Dig. Tech. Pap.*, 2014, 45, 334–337.
- 7 R. Komatsu, R. Nakazato, T. Sasaki, A. Suzuki, N. Senda, T. Kawata, Y. Jimbo, T. Aoyama, N. Ohno, S. Kawashima, H. Ikeda, S. Eguchi, Y. Hirakata, S. Yamazaki, T. Shiraishi, S. Yasumoto, M. Nakada, M. Sato, C. Bower, D. Cotton, A. Matthews, P. Andrew, C. Gheorghiu and J. Bergquist, *J. Soc. Inf. Disp.*, 2015, 23, 41–49.
- 8 S. Hong, J. Yoo, C. Jeon, C. Kang, J. Lee, J. Ryu, B. Ahn and S. Yeo, *Inf. Disp.*, 2015, 31, 6–11.
- 9 S. Park, G. Wang, B. Cho, Y. Kim, S. Song, Y. Ji, M.-H. Yoon and T. Lee, *Nat. Nanotechnol.*, 2012, 7, 438–442.

- 10 D. Kim, H. Kim, W. Jeon, H.-J. Kim, J. Choi, Y. Kim and M. S. Kwon, *Adv. Mater.*, 2024, **36**, 2309891.
- 11 L. Li, L. Han, H. Hu and R. Zhang, *Mater. Adv.*, 2023, **4**, 726–746.
- 12 P. Youngjoo, K. Junkyu, K. Daewhan, L. Seokju, H. Daihyun and S. K. Min, *Soft Sci.*, 2024, **4**, 28.
- 13 T. Lee, J. Kim, J. Lee and H. Kim, *Hybrid Nanomaterials-Flexible Electronics Materials*, IntechOpen, London, 2019.
- 14 J. H. Lee, J. Park, M. H. Myung, M.-J. Baek, H.-S. Kim and D. W. Lee, *Chem. Eng. J.*, 2021, **406**, 126800.
- 15 D. Lim, M.-J. Baek, H.-S. Kim, C. Baig and D. W. Lee, *Chem. Eng. J.*, 2022, **437**, 135390.
- 16 J.-H. Back, D. Baek, K.-B. Sim, G.-Y. Oh, S.-W. Jang, H.-J. Kim and Y. Kim, *Ind. Eng. Chem. Res.*, 2019, **58**, 4331–4340.
- 17 X. Fan, N. Wang, J. Wang, B. Xu and F. Yan, *Mater. Chem. Front.*, 2018, **2**, 355–361.
- 18 H. Park, D. Lim, G. Lee, M.-J. Baek and D. W. Lee, *Adv. Funct. Mater.*, 2023, **33**, 2305750.
- 19 J.-H. Lee, T.-H. Lee, K.-S. Shim, J.-W. Park, H.-J. Kim, Y. Kim and S. Jung, *Int. J. Adhes. Adhes.*, 2017, **74**, 137–143.
- 20 J. O. Akindoyo, M. D. H. Beg, S. Ghazali, M. R. Islam, N. Jeyaratnam and A. R. Yuvaraj, *RSC Adv.*, 2016, **6**, 114453–114482.
- 21 E. Scrinzi, S. Rossi, F. Deflorian and C. Zanella, *Prog. Org. Coat.*, 2011, **72**, 81–87.
- 22 E. A. Papaj, D. J. Mills and S. S. Jamali, *Prog. Org. Coat.*, 2014, **77**, 2086–2090.
- 23 D. E. Fiori, *Prog. Org. Coat.*, 1997, **32**, 65–71.
- 24 A. Gomez-Lopez, S. Panchireddy, B. Grignard, I. Calvo, C. Jérôme, C. Detrembleur and H. Sardón, *ACS Sustainable Chem. Eng.*, 2021, **9**, 9541–9562.
- 25 S. D. Desai, J. V. Patel and V. K. Sinha, *Int. J. Adhes. Adhes.*, 2003, **23**, 393–399.
- 26 K. P. Somani, S. S. Kansara, N. K. Patel and A. K. Rakshit, *Int. J. Adhes. Adhes.*, 2003, **23**, 269–275.
- 27 H. Ding, C. Xia, J. Wang, C. Wang and F. Chu, *J. Mater. Sci.*, 2016, **51**, 5008–5018.
- 28 J. Zheng, R. Ozisik and R. W. Siegel, *Polymer*, 2006, **47**, 7786–7794.
- 29 E. M. Christenson, J. M. Anderson, A. Hiltner and E. Baer, *Polymer*, 2005, **46**, 11744–11754.
- 30 G. Romero-Sabat, L. A. Granda and S. Medel, *Mater. Adv.*, 2022, **3**, 5118–5130.
- 31 B. Sun, H. Wang, Y. Fan, X. Chu, S. Liu, S. Zhao and M. Zhao, *Prog. Org. Coat.*, 2022, **163**, 106680.
- 32 Y. Yuan, Y. Zhang, X. Fu, L. Jiang, Z. Liu, K. Hu, B. Wu, J. Lei and C. Zhou, *RSC Adv.*, 2016, **6**, 83688–83696.
- 33 W. C. Seok, J. H. Park and H. J. Song, *J. Ind. Eng. Chem.*, 2022, **111**, 98–110.
- 34 I. Pinnau, A. Morisato and Z. He, *Macromolecules*, 2004, **37**, 2823–2828.
- 35 P. McCluskey, F. Lilie, O. Beysser and A. Gallo, *Microelectron. Reliab.*, 1998, **38**, 1829–1834.
- 36 E. P. Chang, *J. Adhes.*, 1991, **34**, 189–200.
- 37 J. Zhang, G. Pu, M. R. Dubay, Y. Zhao and S. J. Severtson, *J. Mater. Chem. C*, 2013, **1**, 1080–1086.
- 38 T. R. Ewert, A. M. Mannion, M. L. Coughlin, C. W. Macosko and F. S. Bates, *J. Rheol.*, 2018, **62**, 161–170.
- 39 J. H. Lee, M. H. Myung, M. J. Baek, H.-S. Kim and D. W. Lee, *Polym. Test.*, 2019, **76**, 305–311.
- 40 J. H. Lee and D. W. Lee, *Appl. Surf. Sci.*, 2020, **500**, 144246.
- 41 H.-S. Joo, H.-S. Do, Y.-J. Park and H.-J. Kim, *J. Adhes. Sci. Technol.*, 2006, **20**, 1573–1594.
- 42 J. Kajtna, U. Šebenik and M. Krajnc, *Int. J. Adhes. Adhes.*, 2014, **49**, 18–25.
- 43 M. Zhu, Z. Cao, H. Zhou, Y. Xie, G. Li, N. Wang, Y. Liu, L. He and X. Qu, *RSC Adv.*, 2020, **10**, 10277–10284.
- 44 G.-S. Shim, J.-S. Kim and H.-J. Kim, *J. Ind. Eng. Chem.*, 2020, **89**, 139–146.
- 45 G.-S. Shim, J.-S. Kim, J.-H. Back, S.-W. Jang, J.-W. Park, H.-J. Kim, J.-S. Choi and J.-S. Yeom, *Int. J. Adhes. Adhes.*, 2020, **96**, 102445.
- 46 J.-H. Back, D. Baek, J.-W. Park, H.-J. Kim, J.-Y. Jang and S.-J. Lee, *Int. J. Adhes. Adhes.*, 2020, **99**, 102558.
- 47 H.-W. Park, H.-S. Seo, J.-H. Lee and S. Shin, *Eur. Polym. J.*, 2020, **137**, 109949.
- 48 Z. Cao, Y. Wang, H. Wang, C. Ma, H. Li, J. Zheng, J. Wu and G. Huang, *Polym. Chem.*, 2019, **10**, 3503–3513.
- 49 Y. Shangguan, J. Yang and Q. Zheng, *RSC Adv.*, 2017, **7**, 15978–15985.
- 50 C. MacKenzie and J. Scanlan, *Polymer*, 1984, **25**, 559–568.
- 51 S.-Q. Wang, S. Ravindranath, Y. Wang and P. Boukany, *J. Chem. Phys.*, 2007, **127**, 064903.
- 52 P. E. Boukany, S.-Q. Wang and X. Wang, *Macromolecules*, 2009, **42**, 6261–6269.
- 53 Y. Chen, L. Han, D. Ju, T. Liu and L. Dong, *Polymer*, 2018, **140**, 47–55.
- 54 H. Xia, M. Song, Z. Zhang and M. Richardson, *J. Appl. Polym. Sci.*, 2007, **103**, 2992–3002.
- 55 K. P. Nair, V. Breedveld and M. Weck, *Macromolecules*, 2008, **41**, 3429–3438.
- 56 R. Du, Z. Xu, C. Zhu, Y. Jiang, H. Yan, H.-C. Wu, O. Vardoulis, Y. Cai, X. Zhu, Z. Bao, Q. Zhang and X. Jia, *Adv. Funct. Mater.*, 2020, **30**, 1907139.